Deutsches Zentrum für Luft- und Raumfahrt (DLR), Institut für Physik der Atmosphäre, Oberpfaffenhofen, Germany

Development and propagation of severe thunderstorms in the Upper Danube catchment area: Towards an integrated nowcasting and forecasting system using real-time data and high-resolution simulations

A. Tafferner, C. Forster, M. Hagen, C. Keil, T. Zinner, H. Volkert

With 15 Figures

Summary

Quickly developing and fast propagating thunderstorms are an important source of high impact weather (sudden occurrence of high precipitation rates and high wind speed) in central Europe. The region to the north of the Alps is particularly prone to such natural threats. Possibilities how to combine data from routine observations taken by geostationary satellites, a ground based radar network and lighting detection systems with high resolution forecast data for routine nowcasting purposes are exemplified for a typical summer situation of August 2004. The gradual development of the different technologies is sketched and a vision of how to combine the various data and forecasting sources is presented.

1. Introduction

Floods are next to storms the most important geophysical events which regularly cause losses of life and property. The demand to mitigate the impact of these effects calls for preparation. Essential features are early warning systems and effective emergency planning (Kron 2004).

Traditionally flood warnings use real time observations of river levels upstream and empirical or physical modelling of the time-dependent discharge along the river in question. Near-real time monitoring of the areal precipitation by the help of precipitation radar networks allowed increasing the forecast horizon by a few hours. Longer lead times necessitate the use of precipitation data from the output of high-resolution numerical weather prediction (NWP) models. The atmospheric components of this quite complicated chain of events were systematically investigated during the European project HERA (**He**avy p**r**ecipitation in the **A**lpine region; cf. Volkert 2000, and references therein). The long chain from forecasting and analyzing in near-real-time atmospheric precipitation and the linkage to hydrological warnings for medium and larger scale catchments was recently reviewed with a special focus on the eastern Alpine region (Cegnar and Rakovec 2005). The linking of atmospheric and hydrological numerical forecasting in mountainous terrain was demonstrated for the Lago Maggiore area (Ranzi et al. 2007) in the framework of a large field campaign (Volkert and Gutermann 2007).

Correspondence: Arnold Tafferner, Deutsches Zentrum für Luft- und Raumfahrt (DLR), Institut für Physik der Atmosphäre, Oberpfaffenhofen, 82234 Wessling, Germany (E-mail: arnold.tafferner@dlr.de)

For hydrology the natural spatial structure is given by river catchments upstream of a certain location along a river. This study concentrates on the upper Danube catchment (UDC) upstream of Vienna. This choice was made for a number of reasons: (*i*) the catchment size of some $80,000\,\text{km}^2$ is sufficiently large for a promising pilot application, (*ii*) the region is an integral part of the CADSES (Central, Adriatic, Danubian and South-Eastern European Space) region as defined by the EU neighbourhood programmes (cf. www.cadses.net), (*iii*) the region is well equipped with routine and research instruments, (*iv*) sufficiently severe events happen over the region reasonably often, and (*v*) previous studies are available that can be used as starting point for an unifying approach. The UDC is irregularly shaped (as any river catchment) and crossed by the Danube in an asymmetric way (Fig. 1). It is bounded by the low mountain ranges (in German: *Mittelgebirge*) Swabian(-Franconian) Alb, where the Danube has its source, and Bavarian Forest in the north and the northern half of the eastern Alps to the south. The largest part of the UDC area is covered by the northern Alpine forelands from near the Lake of Constance in the west to the Viennese

Woods in the east. The extension of the UDC is about $720\,\text{km}$ in west–east and $400\,\text{km}$ in south–north directions. This area at the right bank of the upper Danube is taken as the focus for this study. The UDC covers approximately 10% of the area of the entire Danube catchment $(817,000\,\text{km}^2)$, which is by far the largest of the European river systems and shared by no less than ten countries and a central element of CADSES. The situation of the UDC relative to the catchments of the other larger river systems in central Europe is given in Fig. 2 (white areas around the Adriatic depict smaller catchments draining directly to the sea).

This study concentrates on summertime thunderstorms as a notoriously difficult to forecast source of often heavy precipitation. Remote sensing data from geostationary satellites and ground based radar networks are combined with high-resolution NWP results. The data sources are presented in the next section. Sample results from a recent case study are presented in Sect. 3 to exemplify our approach. A more general estimate of the potential of system components for nowcasting and forecasting is given in Sect. 4. The potential of an integrated system as a concrete vision for the future concludes the presentation.

Fig. 1. Satellite view of the upper Danube catchment (UDC) upstream of Vienna. The approximate boundaries to the neighbouring major European-scale river catchments of Rhine, Elbe, Po, Adige and Drau are dotted. Important orographic features at the edges of UDC are the northern parts of the Eastern Alps in the south and Swabian Alb and Bavarian Forest in the north. The major part of the UDC drainage area consists of the northern Alpine forelands with Munich in its centre and the polarimetric radar location at DLR-Oberpfaffenhofen south-west of it. This rectangle on a stereographic weather map projection (vertical meridian at $10°E$) is used as nowcasting domain in this study. The extension of the UDC is about $720\,\text{km}$ in west–east and $400\,\text{km}$ in south–north directions

Fig. 2. Situation of the upper Danube catchment (UDC) and the extent of Fig. 1 (dotted rectangle) within the European scale catchments of major rivers (in grey). The locations of Munich (M) and Vienna (V) are given to ease the orientation. (Map adapted from the Wikipedia online dictionary)

2. Data sources

The synoptic view on and the linkage of different data sources is at the heart of meteorological analysis and prognosis since more than 80 years. Bergeron (1928) assembles a variety of older explorative studies (*loc. Cit.,* pp. 11–15), stresses the necessity of daily routine applications and shows how the wealth of different measurements and qualitative observations can be blended together to obtain a consistent picture of the current weather and its development during the following hours. This study makes use of routine surface observations combined with remote sensing data from geostationary satellites, lightning detection systems and precipitation radar networks.

Surface data are used in two ways. Time series of precipitation rates give an indication about intensity and duration of precipitation at single stations. A novel technique of objectively analyzing data from dense observational networks in complex terrain (VERA: Vienna Enhanced Resolution Analysis; Steinacker et al. 2000b) is nowadays regularly applied for the Alpine region. In the three hourly analyses of synoptic observations (00, 03,..., 21 UTC) the UDC is completely contained (cf. http://www.univie. ac.at/IMG-Wien/vera), while special analyses at the intermediate asynoptic hours are carried out for sub-regions according to the availability of observations.

After the launch of Meteosat-8 in 2002, the first of the Meteosat Second Generation satellites, images from a fixed, e.g., geostationary position are available at 15 min intervals at resolutions between 3 and 1 km. The distinct increase in spatial and temporal resolution opens the way for automatic tracking procedures of regional and small scale cloud systems, e.g., in the context of mesoscale convective complexes (Zinner et al. 2008).

In a similar fashion data from routine networks of precipitation radars can be used to assess the extent of precipitation systems and rain bands as well as for automatic tracking of precipitation cores (Kober and Tafferner 2008). Explorative studies in the northern Alpine foreland were undertaken within project HERA (Hagen et al. 2000). Blending this information with data from a lightning detection systems helps to identify the convectively most active cells (Steinacker et al. 2000a). Data for the LPATS/BLIDS systems are used here.

3. The case of 12 August 2004 put in context

Detailed case studies help to shed light on the scales involved in the formation and development phases of strong precipitating systems as well as on the data types which were available at the time of the analyses. The inspection of prominent cases helps to sharpen the eye of developers for automatic procedures regarding scale interactions and possible complications.

The combination of an orographically accelerated front with strong embedded convection and the technological state of the late 1980ies can be seen from the analyses of the *papal front* which rushed across the north Alpine forelands on 3 May 1987 (Volkert et al. 1991 and references therein). Mesoscale surface data analyses of wind and precipitation rates provided the backbone; reflectivity data from a single radar on film indicated the size of the mesoscale convective complex; European scale numerical model analyses gave the large scale forcing; high resolution modelling including a realistic simulation of precipitation processes was still in its infancy.

The four day precipitation event of 5–8 July 1996 was investigated in detail during project HERA, including hindcast simulations with the *Deutschland-Modell*, the then operational forecasting tool of Deutscher Wetterdienst (Keil and Volkert 2000). A comparison concerning 24 h precipitation amounts at single stations and the areal extent of precipitation regions (from radar imagery) showed promising skill, although the model's horizontal mesh-size of 14 km was still very coarse. Nevertheless a special investigation concerned the *Isar-Amper* watershed upstream of Freising, a third order catchment in the southern part of UDC.

Now we apply current observational and simulation tools for a case of August 2004 when a large thunderstorm complex was generated over southwest Germany ahead of an advancing cold front. This mesoscale convective complex had a lifetime of some 6 h (1500–2100 UTC). At 15 UTC a zone of strong decrease in surface pressure (-2.5 hPa/3 h) was followed within 250 km by a belt of equally fast pressure rise
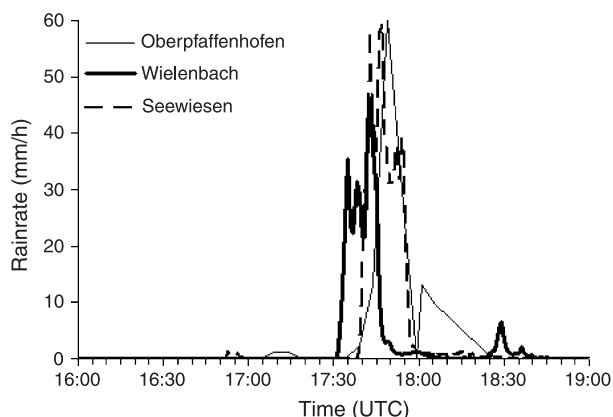
Fig. 3. Quasi-synchronous onset of short duration downpours at three stations to the southwest of Munich on 12 August 2004

ue for Oberpfaffenhofen at 18:00 is likely to be a single erroneous data-point). The short scale pressure gradient between Munich city and Munich international airport $(5.6\,\text{hPa}/28.6\,\text{km} \approx 20\,\text{hPa}/100\,\text{km})$ is a further indicator of the vigour of the system.

When routine surface observations of wind and humidity are interpolated on a regular grid by taking into account structure functions that depends on the regional topography (Steinacker et al. 2000b), lines of strong convergence of both mass and moisture can be objectively determined (Fig. 4). The red area to the east of 10°E designates convergence values equivalent to a transport of $20\,\text{g/kg}$ moisture with $10\,\text{m/s}$ over 100 km. Such zones are prone to fast development of strong convection and eventually also heavy precipitation. Although the absolute precipitation amount was not very significant, this case allows well to exemplify the potential of remote sensing tools for the detection of potentially
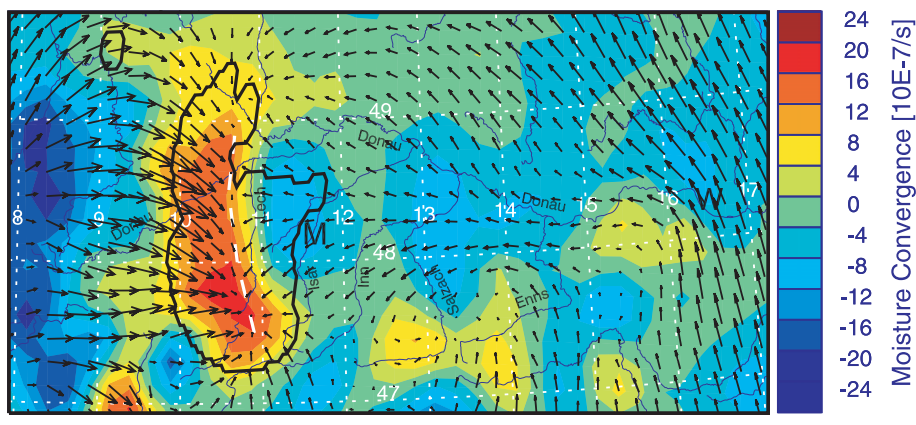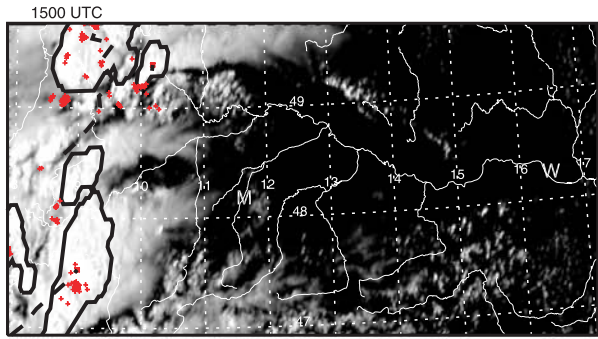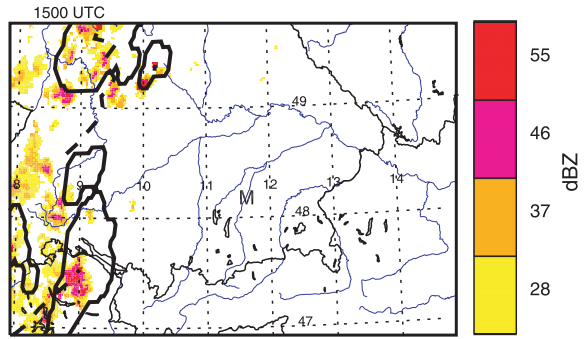
$(2.5\,\text{hPa}/3\,\text{h})$. During the rapid movement towards the northeast strong wind gusts (up to $30\,\text{m/s}$) occurred accompanied by an abrupt onset of short duration downpours exceeding precipitation rates of $50\,\text{mm/h}$ (Fig. 3; the zero-val-

Fig. 4. Objective gridded analysis of surface data (VERA technique) for 17 UTC on 12 August 2004: moisture flux divergence in colour in units of $10^{-7}\,\text{kg}/(\text{kg s})$, or $10^{-4}\,\text{g}/(\text{kg s})$, and surface winds (the vector below the figure indicates 10 m/s). The white line marks the squall line where winds are converging from opposite directions and likely to trigger strong vertical motion; the black line designates the boundary of the convective complex (cf. Fig. 5); Munich and Vienna are marked by M and W; the names of rivers in the northern pre-Alpine forelands are given in German
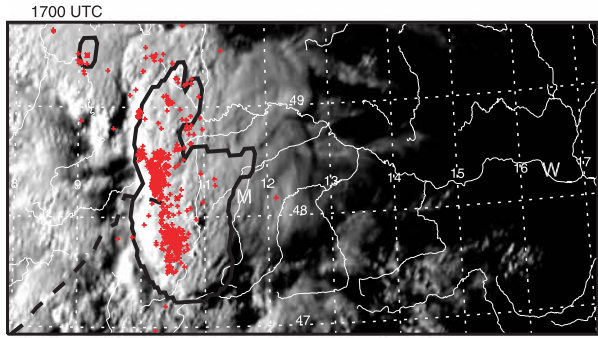
Fig. 5. Development and progression of a precipitating mesoscale convective complex across the upper Danube catchment during the afternoon of 12 August 2004 as observed by three different observational systems. Left column: cloud structures in the high resolution visible channel (**a**, **b**) and water vapour channel (6.2 μm) of Meteosat-8 (**c–e**; scales of white) and total lightning within 5 minutes before observation time (crosses). Right column: radar reflectivies of precipitation cores (>28 dBZ, scale in **f**) adapted from the European radar composite of *Deutscher Wetterdienst*). In all frames thick black lines mark boundaries of convective cells objectively determined from satellite data by Cb-TRAM at the given time and dashed black lines indicate the paths of the centre of major convective complexes during the previous hours. In figure **j**, the boundary of a major precipitation cell as detected by the Rad-TRAM together with the path during the previous hours is indicated by black lines, too. Rivers and the dotted $1° \times 1°$ grid on a stereographic weather chart projection aid the orientation; M: Munich; W: Wien (Vienna)
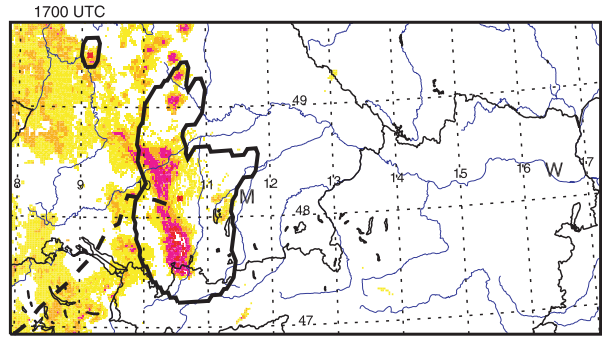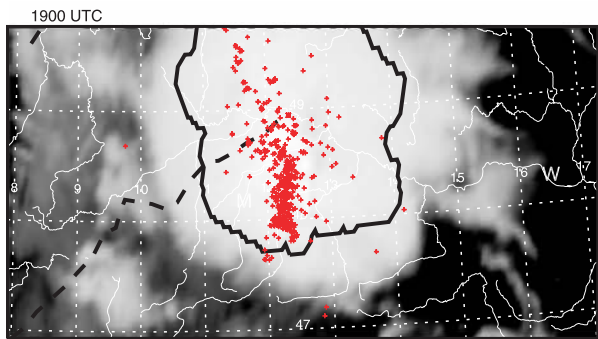
a 1500 UTC
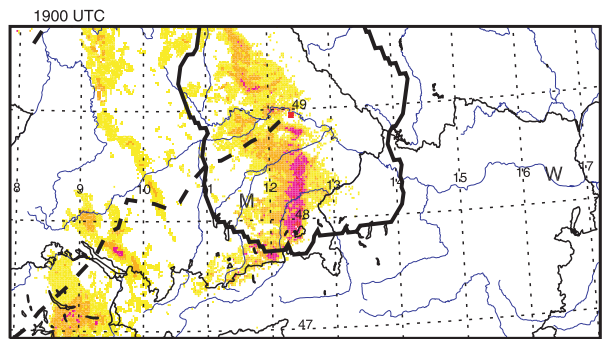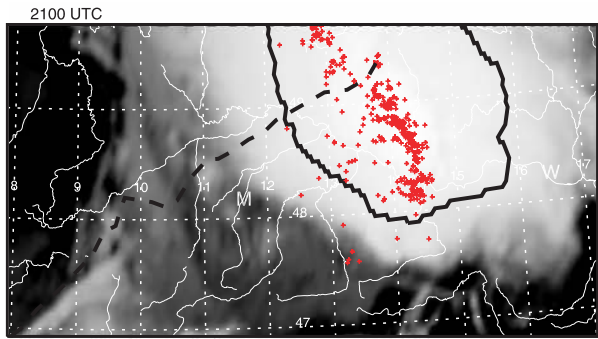**b** 1700 UTC
c 1900 UTC
d 2100 UTC
e 2300 UTC
f 1500 UTC
g 1700 UTC
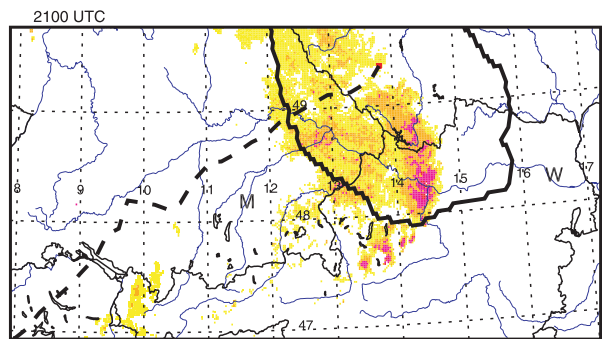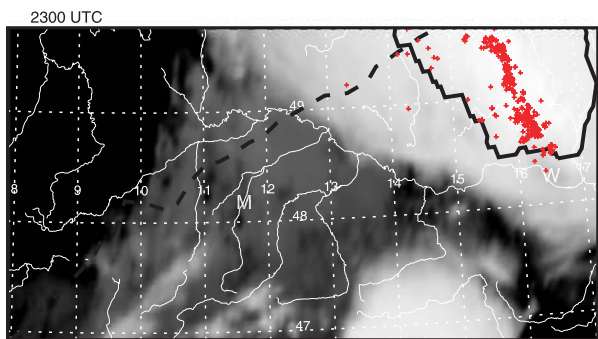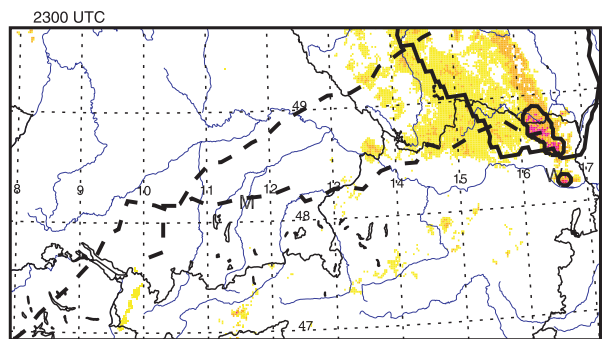**h** 1900 UTC
i 2100 UTC
j 2300 UTC

dBZ

55

46

37

28

dangerous situations. Let us now turn to different remote sensing systems and their superposition in a common regional weather chart projection.

The development and progression of the top of cloud systems is routinely monitored through the use of satellite imagery from the Meteosat second generation family. Active thunderstorms can be traced by areal plots of lightning locations, while the extent of precipitation areas is regularly determined from reflectivity composites obtained by precipitation radar networks. Figure 5 composes all three kinds of remote sensing data in parallel columns for the eight hour period 15 to 23 UTC on 12 August 2004. Black solid lines in all sub-figures a–j mark the boundary of mature convective cells as detected by the cloud tracker Cb-TRAM (Zinner et al. 2008). The detection algorithm uses a combination of the infrared 10.8, the 6.2 μm (water vapour) and the high resolution visible channel (HRV) in order to discriminate three phases of convective cells: initiation, rapid cooling and mature (only these are shown in Fig. 5). The cloud cells are tracked by using a displacement vector field derived from an image matching procedure (for details the reader is referred to Zinner et al. 2008). The corresponding tracks of the cloud centres are marked in Fig. 5 by dashed lines for cells which exist longer than one time step, i.e. 15 min. Total lightning is plotted for all occurrences during the past 5 min before observation time; e.g. 900 flashes during the 1655–1700 interval. The superposition of the various data reveals: (*i*) the convective complexes progressed from south-west to northeast with an average speed of about 65 km/h, (*ii*) during the first two hours (Fig. 5a, b, f, g) several smaller cells merged into one major system which increased in intensity and reached its maximum at 17 UTC as indicated by the lightning observation density and radar reflectivity values, (*iii*) after 17 UTC the system continued to exist with decreased but unchanged intensity until late in the evening (Fig. 5e, j), (*iv*) the severe precipitation only covered small portions of the overall convective complex, and (*v*) lightning observations were concentrated in the regions of maximum radar reflectivity, however, single flashes also occured within the region of the thunderstorm cloud anvil and well within the contour of the Cb-TRAM cell. These observations are most likely attributable to intra-cloud discharges.

Note that Fig. 5a and b contain as background the HRV Meteosat-8 image which is also used in Cb-TRAM at these times in order to better confine the thunderstorm cloud within the convective updraft region (cloud "roughness" in the HRV). At later times, i.e. after sunset within the domain treated by Cb-TRAM, the HRV channel cannot be used and, thus, the detected cloud region gets enlarged. High precipitation cores with reflectivity greater than 37 dBZ are almost always found well within the convective clouds as detected by Cb-TRAM. There are some areas with reflectivity exceeding 37 dBZ which are not covered by Cb-TRAM clouds. Those are, however, also lacking lighting observations. Remarkably, the convective features can be tracked for long time intervals. Figure 5j shows the combined result from cloud and radar trackers, the latter applied with a threshold of 37 dBZ. Apparently, both trackers were able to trace the cloud complex and the precipitation cell in parallel for more than 6 h during their propagation through the UDC. Rad-TRAM uses the same tracking algorithm as the cloud tracker, with the European radar composite as data base (details in Sect. 4.2 and in Kober and Tafferner 2008).

Retrievals from the polarimetric radar POLDIRAD at DLR Oberpfaffenhofen provide additional insights although they are not yet available on a routine basis. At 1658 UTC the main shaft of high reflectivity extends up to more than 14 km above ground with a width of about 10 km (red colour range in Fig. 6, left). A classification of hydrometeors (Fig. 6, right) reveals that this region is in essence composed of wet graupel (yellow) above dry hail (orange) at the leading edge and large raindrops behind (dark blue). A horizontal scan across the sector west of Oberpfaffenhofen at a low elevation (1°) allows to retrieve instantaneous rate rain from polarimetric measurements (Fig. 7). This adds quantitative detail to the larger overview shown in Fig. 5.

More generally it becomes obvious that the detection and regular monitoring of such a convective system in near real-time carries potential for nowcasting purposes and warning schemes. We now attempt a quantification of this potential using a combination of nowcasting (up to 1 h ahead) and forecasting schemes (several hours ahead).
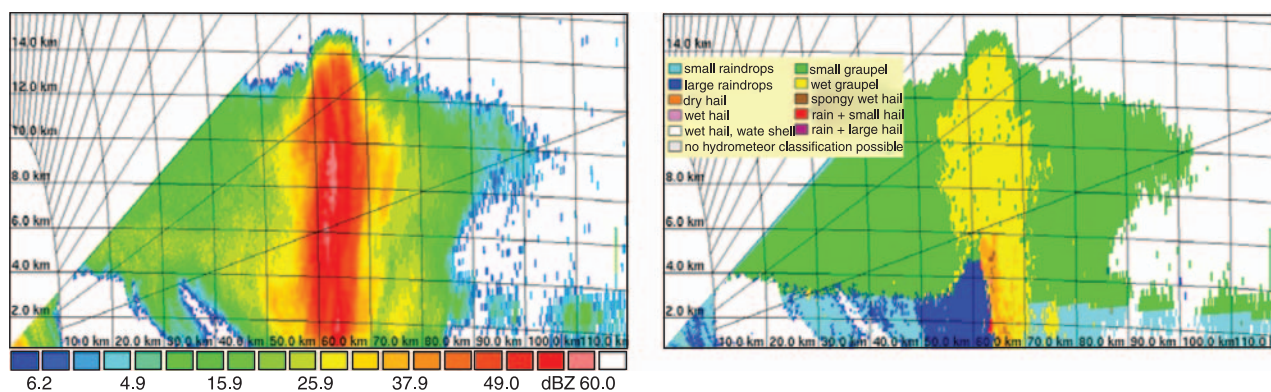
| 6.2 | 4.9 | 15.9 | 25.9 | 37.9 | 49.0 | dBZ 60.0 |

Fig. 6. Cross-section at 1658 UTC on 12 August 2004 towards SW (240°) through an approaching thunderstorm with the polarimetric radar POLIDRAD at DLR Oberpfaffenhofen: reflectivity (left) and hydrometeor classification (10 classes) from various combinations of polarimetric data (right)
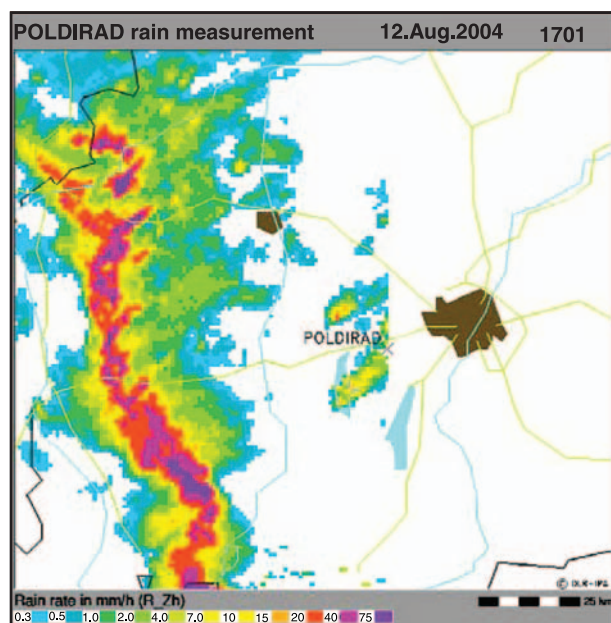

Fig. 7. Instantaneous rainrate (mm/h) in the sector west of Munich (large patch), determined from polarimetric measurements at 1701 UTC on 12 August 2004; radar beam elevation: 1°; pixel size: 1 km × 1 km

4. Nowcasting and forecasting

Short term forecasting of severe weather phenomena and issuing appropriate warnings is particularly important for timely planning of risk prevention measures by public authorities and the private sector. These high impact weather features are however difficult to predict. On one hand they are often short-lived and of small scale. On the other hand, also longer living, propagating convective systems undergo various phases during their life cycle, from rapid development over mature phase to decay, i.e. there exist complex dynamical and micro-physical processes which cannot be detected by current routine observation systems, at least not to the desired level of detail. Furthermore, convective complexes may split or merge which complicates the whole process even more. Due to the lack of initial data which describe accurately the state of the atmosphere on small scales, it is understandable that numerically forecasting such weather features correctly in space and time will often fail, despite high spatial grid resolution and elaborate model physics. The success of such forecasts, at least on a routine basis, is therefore often a matter of good fortune, at least for time scales exceeding 60 min.

Therefore, present nowcasting efforts rely mostly on techniques based on extrapolation of recent observations in time. Various nowcasting systems have been developed over the past 20 years based on such an approach using primarily remote sensing data from radar, satellite and lightning (e.g., Dixon and Wiener 1993; Handwerker 2002; Morel and Sénési 2002; Mueller et al. 2003). A status report on nowcasting thunderstorms is presented in the work of Wilson et al. (1998).

For the upper Danube catchment area, we present for the thunderstorm outbreak of 12 August 2004, nowcasting examples using the tools available at the Institut für Physik der Atmosphäre of the Deutsches Zentrum für Luft- und Raumfahrt (DLR). These comprise a *cloud tracker*, a *radar tracker* and high resolution *numerical forecasting model*.

4.1 Nowcasting with the cloud tracker

The cloud tracker Cb-TRAM is not only used for tracking and monitoring convective clouds, but also to extrapolate the cloud's position and size up to one hour ahead in time by applying a displacement vector field of an area-based image matcher. This vector field, defined at each pixel position of the image and often called "optical flow", describes the warping of one image into the subsequent one in such a way that either the difference of the image intensities is minimised (classical optical flow; used here in Cb-TRAM) or that the local correlation is maximised (Zinner et al. 2008). As an example we show CB-TRAM results for the thunderstorm propagating across the upper Danube catchment in the afternoon of
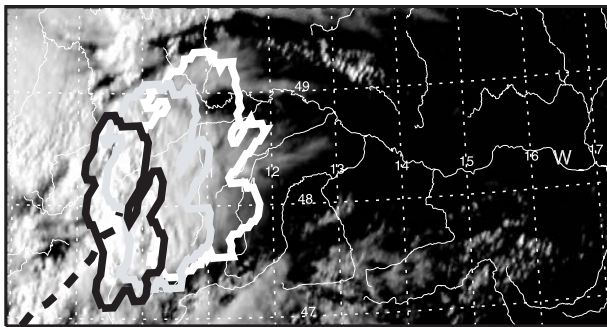

Fig. 8. Example of nowcast provided by cloud tracker Cb-TRAM. Detected mature convective complex (black contour) at 12 August 2004, 16 UTC superimposed with high resolution visible image of Meteosat-8 over the UDC. Grey and white contours mark the 30 and 60 min extrapolated nowcast positions of the convective cells. Dashed black line denotes the previous track of the cell centre

12 August 2004. In Fig. 8, the black contour marks the outlines of the major thunderstorm cell detected at 16 UTC. The high resolution visible image from Meteosat 8 is chosen as background. Also displayed is the track of this cell and extrapolations for 30 and 60 min, respectively.

A comparison between the 60-min-nowcast with the next analysis at 17 UTC (Fig. 5g) reveals a good agreement in the overall position. At most edges of the convective complex, nowcasted and analyzed position are in accord, while the largest difference is found at its the north-eastern flank. Having in mind the uncertainties inherent in both, detection and extrapolation techniques for convective systems these results are promising indeed. Further tests on the nowcasting performance of Cb-TRAM have been undertaken for other pilot case-studies with promising results (Kober and Tafferner 2008).

4.2 Nowcasting with the radar tracker

The radar tracker Rad-TRAM is another, analogously novel tool at DLR (Kober and Tafferner 2008). Based on the same algorithms for detection and tracking image features as the cloud tracker CB-TRAM, the threshold for detection of severe weather objects is adjusted to reflectivity values used in radar imagery. Specifically, the European radar composite provided by the German Weather Service DWD was used and a threshold of 37 dBZ was chosen for the detection of severe weather objects with heavy precipitation.

Results for the maturation phase of the thunderstorm (1600–1700 UT) are given in Fig. 9.
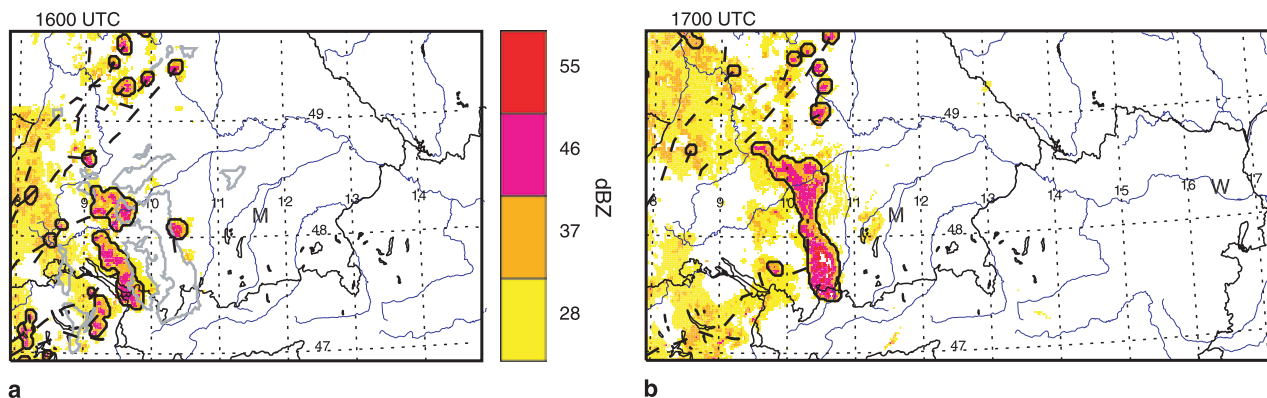

Fig. 9. Radar composite at 16 UTC (**a**) and 17 UTC (**b**) in shades of grey above 28 dBZ (scale given in (**a**)) with superimposed contours marking heavy precipitation above 37 dBZ as determined by Rad-TRAM (bold lines), previous paths of the cells marked with dashed lines. Extrapolated nowcast positions further to the east 60 min later are given in (**a**)

The positions of various cells detected by Rad-TRAM are displayed by thick black contours alongside with the one-hour extrapolations marked by closed grey contours further to the east. The European radar composite is shown as background in grey shading for four reflectivity calsses exceeding 28 dBZ. Also plotted are the tracks of these three cells indicating that these are longer lived features propagating with the thunderstorm line (cf. Fig. 5). Note that the forecast cells are not simply a linear translation of the detected cells, as their shapes varying with time indicate. The extrapolated cells result from the pyramidal image matcher which produces displacement vectors for all identified pixels within each cell, dependent on the scales of images features as in Cb-TRAM.

A comparison of the one-hourly extrapolation with the observation at 17 UTC we find agreement in most cell positions and a combination of two cells into one (cf. also to the radar image in Fig. 5g at this time). Obviously, these cells have merged. Correspondingly, the track of the combined cell is rather short, as the radar tracker has identified it as a new cell which did not inherit either one of the previous cells. Note however, that this cell will continue to exist at least for six hours (corresponding track in Fig. 5j). Comparing the locations of the extrapolated with the locations of the observed cell more closely we find a better overlap in the southern part, white its northern part coincides only with half

of that of the extrapolated cell. Nevertheless, as the time span of 60 min is quite long for propagating cells under development, we consider the result as promising for nowcasting purposes. As in the case of nowcasting with Cb-TRAM, further tests including statistical verification measures were successfully undertaken (Kober and Tafferner 2008).

4.3 Forecasting with numerical model

As noted above, high resolution numerical modelling can be successful for forecasting thunderstorms if fitting initial and boundary conditions are available. Here we present an example of direct numerical forecasting of the thunderstorm evolution during 12 August 2004.

For the forecasting of environmental meteorological parameters in small-scale areas, especially around airports, a model chain for real-time execution, named NOWVIV, has been set up at DLR. It consists of a research-version of the MM5/FSL high resolution model (Grell et al. 2000) and the operational Lokal-Modell of the Deutscher Wetterdienst (DWD, Doms and Schättler 1999), the latter providing initial and boundary conditions. Figure 10 shows the model domains: the operational domain of the LM (version 1) and two nested MM5 domains with resolutions of 6.3 and 2.1 km, respectively. In the vertical, 50 levels are selected for the MM5 with particular high resolution of the boundary layer,
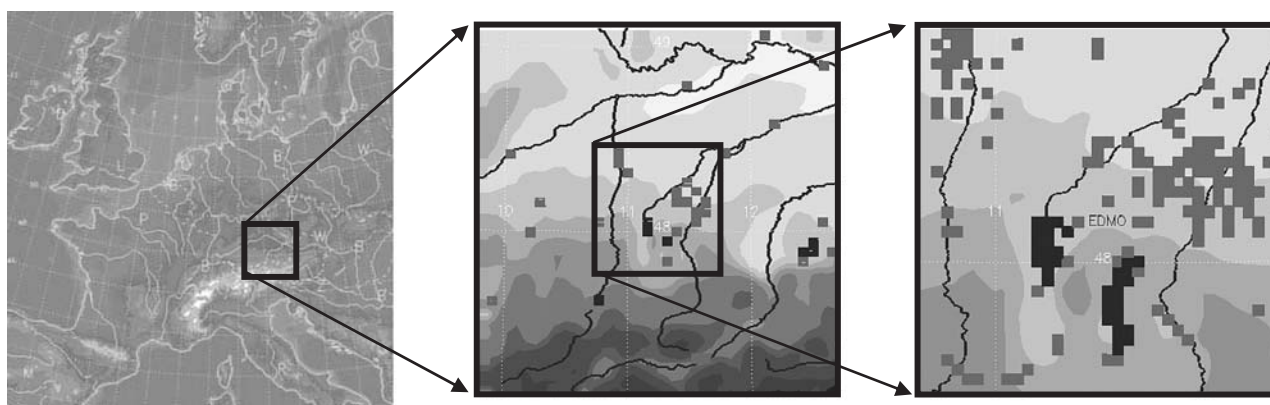
Fig. 10. Nested model domains of the NOWVIV system: Central Europe covered by the Lokal Modell (LM1) of DWD with location of MM5/FSL outer domain (left); outer MM5 domain over the central UDC with location of inner domain (middle); inner MM5 domain centred at Oberpfaffenhofen airport (EDMO) and covering the area between rivers Lech and Isar (right). Grey shading represents the orography (dark shading higher elevation), small squares indicate land use type "urban", also indicating the size of a grid box. The extensions of the domains from left to right are approximately: 2200 km, 240 km, 80 km

starting with 8 m at the ground and increasing to about 100 m at a height of 2 km. Special care was taken to provide representative orography, land-use and soil type data at the model resolution, as these parameters have a profound influence on the surface energy and momentum balance and, thus, also on the diurnal evolution of the boundary layer.

Model runs are carried out with a full physics package, i.e. boundary layer processes, radiation and cloud physics are taken into account, the latter with mixed phases of water including snow, ice and graupel. Details on NOWVIV can be found in Gerz et al. (2005) and (Frech et al. 2007).

For the 12 August 2004 thunderstorm passage, the model was initialized with standard output data from the operational LM forecast run starting at 12 UTC on 12 August 2004. No further assimilation of local data, e.g. from radar, has been carried out so far. Figure 11 presents a graphical depiction of the model forecast thunderstorm development for 19 UTC after 7 h of forecast. The squall line ahead of the towering cumulus clouds is clearly visible by the marked jump in wind strength as indicated by the wind vectors. A thunderstorm at the baseline of the Alps is fully developed as seen from the appearance and distribution of the hydrometeors.

When compared to the observations, e.g. from surface observations at Munich and radar mea-
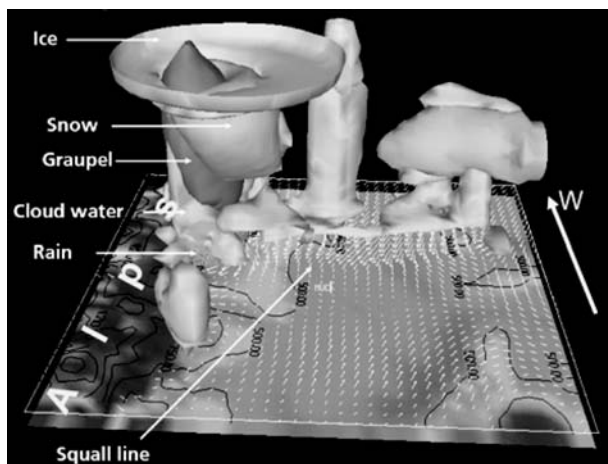

Fig. 11. Hydrometeor distribution and wind field 800 m asl for 12 August 2004, 19 UTC within the outer MM5 domain (cf. Fig. 10 middle); 7 h hindcast simulation in a perspective view from east on the north Alpine foreland which contains the upper Danube catchment.. Note the exaggerated vertical scale (0... 12 km) versus 250 km in the horizontal directions

surements (compare panels in Fig. 5 for 17 UTC and 19 UTC), the passage of the thunderstorm line in this hindcast simulation appears to be about 1.5 h late. Nevertheless, this example documents the significant potential of current numerical models to forecast the evolution and propagation of thunderstorms. Admittedly, this is better possible for cases which are primarily driven by synoptic forcing (as the 12 August 2004). Forecasting the onset and growth of isolated thunderstorms with weak synoptic forcing poses a much more difficult task, as subtle inaccuracies in the initial data, primarily in the distribution of moisture fields, may have a strong impact on location and onset of the convective development.

4.4 Estimating forecast quality

The errors in mesoscale forecasts often take the form of phase errors, where a forecasted weather system is displaced in space or time relative to its counterpart in reality. For such errors, a direct measure of the displacement is likely to be more valuable than traditional measures.

Recently, Keil and Craig (2007) proposed a spatial verification measure that is based on image comparison of observed and forecasted satellite imagery for the geostationary satellite Meteosat-8. This forecast quality measure (FQM) combines the magnitude of a mean displacement vector calculated with a pattern recognition method (Pyramidal Image Matching algorithm) and the final amplitude error of observed and morphed forecast image. The Pyramidal Image Matching algorithm, originally developed to detect cloud features (e.g., convective clouds, contrails) in satellite imagery (Muller et al. 2007; Zinner et al. 2008), combines amplitude-based measures (e.g., correlation coefficient, RMSE) and distance-based measures (e.g., pure binary image comparison) by inter-comparing real valued images at different scales within a fixed search environment. For the application considered here, where imagery of Meteosat-8 IR 10.8 μm channel is used as a proxy to locate precipitating cloud features, a threshold brightness temperature ($BT_{thres} = -20\,°C$) is applied to mask out the land surface and shallow non-precipitating clouds. Since we are primarily interested in quantifying mesoscale position errors of convec-

tive storms that may occur in similar synoptic environments, the coarsest matching scale is confined to sub-synoptic distances of at most a few hundred kilometers. A forecasted and an observed feature that are closer than this distance will be considered to be the same feature, but displaced in space (and a displacement vector will be computed), whereas features separated by larger distances will be assumed to be unrelated.

A displacement vector field is computed which morphs the simulated image into a best match of the observed image. The magnitude of the mean displacement vector gives some indication of the forecast quality, provided that there are features in the fields available to be matched. This information is combined with an amplitude error of observed and morphed forecast brightness temperatures, which gives an indication of whether there are cloud features that have in fact been matched. The metric FQM attains zero for a "perfect" forecast.

Here the FQM is applied evaluating mesoscale forecasts performed with the non-hydrostatic Lokal-Modell (LM, Steppeler et al. 2003). The operational LM domain encompasses central Europe (see, e.g. Fig. 12a; 325×325 grid points with 35 vertical levels) with a horizontal resolution of 7 km. Prognostic precipitation and parameterized moist convection after Tiedtke are used in LM-7-km, while in the new high-resolution LMK with a horizontal resolution of 2.8 km (Fig. 12d) only explicit precipitation is active. Three short range deterministic LM experiments conducted for the 12 August 2004 episode are compared: (*i*) LM with $\Delta x = 7$ km started at 00 UTC (experiment *a01*, Fig. 12b), (*ii*) LM with $\Delta x = 7$ km started at 06 UTC (experiment *a02*, Fig. 12c), and (*iii*) LMK with $\Delta x = 2.8$ km based on experiment *a01* started at 00 UTC (experiment *ak1*, Fig. 12d).

Experiments *a01* and *a02* only differ in the initialisation time, whereas experiment *ak1* has a higher resolution and is nested in LM experiment *a01*. In Fig. 12, the observed and model-forecast synthetic satellite imagery of these three experiments is displayed. The key feature, that
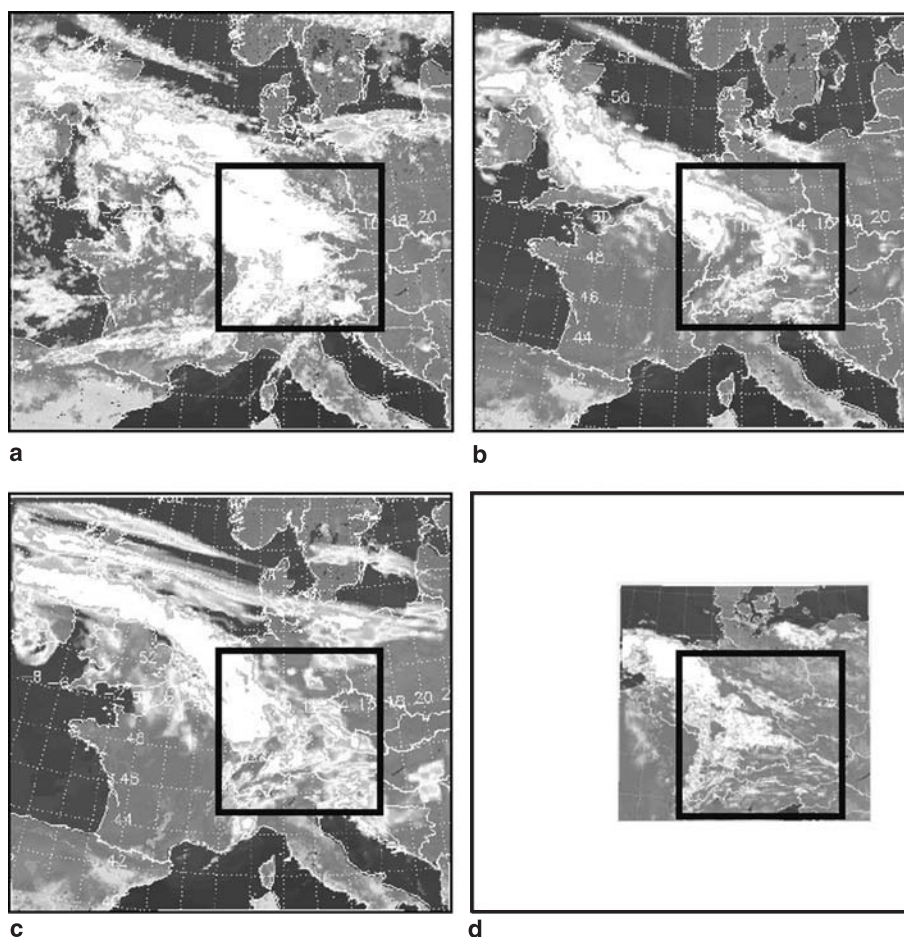
Fig. 12. Comparison of observed and computed cloud structures over central Europe for 12 August 2004, 17 UTC, visualized through their brightness temperature at 10.8 μm. (**a**) data from Meteosat-8; (**b**) 17 h hindcast with LM ($\Delta x = 7$ km) started at 00 UTC; (**c**) 11 h hindcast with LM ($\Delta x = 7$ km) started at 06 UTC; (**d**) 17 h hindcast with LMK over a smaller region ($\Delta x = 2.8$ km) started at 00 UTC. The quality measure (FQM, see Fig. 13) is calculated within the black rectangle

is the cloud system extending from the British Isles to the Alps as shown in the observation (Fig. 12a), is reproduced in all experiments. However, LM underestimates the cloud amount and, particularly, the pre-frontal convective clouds. The position and orientation of the cloud system is best captured in LM experiment *a01* (Fig. 12b) exhibiting convective pre-frontal clouds across Bavaria at 17 UT. LM experiment *a02* (Fig. 12c) produces more clouds than *a01*, but the weather system is slightly lagging behind the observed position and, consequently, compares worse with satellite observations. LMK experiment *ak1* (Fig. 12d), despite operating at higher resolution, strongly underestimates the development of convection between the river Danube and the Alps in southern Bavaria resulting in a mismatch with satellite observation in that region, whereas the location of the cold front along the French German border is nicely reproduced. Calculating the forecast quality measure confirms this visual subjective evaluation.

In Fig. 13, a time series of the FQM is depicted for the period 12 to 23 UTC on 12 Aug 2004. LM experiment *a01* is generally better than *a02*, whereas *ak1* gives slightly lower values. According to FQM, experiment *a01* is better than *a02* at 17 UTC, while the errors in *ak1* compensate in the $900 \times 900 \, \text{km}^2$ region (bad forecast of convection, good forecast of cold front) giving a similar value as for experiment *a02*. All FQM values of the three short-range forecasts peak at
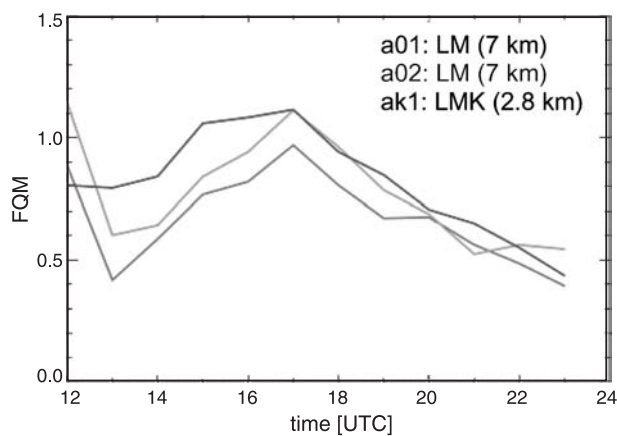
17 UTC indicate the well-known difficulty of mesoscale models to reproduce the spatio-temporal evolution of strong summertime convective activity.

Summarizing, the new quality measure based on image matching of observed and synthetic satellite data provides an objective measure to estimate forecast quality which can be applied to evaluate different numerical forecasts for a certain weather event, which has to contain clouds.

5. Potential of an integrated system

In the previous chapters, we demonstrated how individual cells within a propagating thunderstorm line can be monitored by satellite, radar and lightning data, nowcasted by the cloud and radar trackers CB-TRAM and Rad-TRAM and forecasted by high-resolution numerical weather prediction models. Furthermore, algorithms are able to derive rain rate and hydrometeor type from radar observations.

Generally these tools have been designed individually for a particular purpose independent of one another. Combining these within one integrated system can be expected to provide a greatly enhanced benefit in monitoring and nowcasting capability, i.e. an integrated system can process and contrast the assertions of the individual tools, e.g. as regards to the exact location of a particular weather system, its intensity and movement, and thus provide a more reliable assertion of the future state of a weather system as when only one data source or nowcasting tool were used.

Integrated systems have already been installed for particular purposes, e.g. for providing weather informational products for improving air terminal planning as realized in the Integrated Terminal Weather System (ITWS) for several US airports (Evans and Ducot 1994). A co-operation among the weather services of Germany, Switzerland, Denmark and Canada has been established to design a workstation based interactive graphical user interface for the display of all kind of meteorological data including the output from numerical models and nowcasting applications (Koppert 2002). This system, named NINJO, has meanwhile been established at forecasting offices in Germany. For nowcasting significant weather objects, the blending

Fig. 13. Time series of forecast quality measure (FQM) during the second half of 12 August 2004 for three deterministic simulations of the Lokal Modell (LM) evaluated for the marked area indicated in Fig. 12

of data from surface observations and from the French radar network has been realized at Meteo-France within an operational environment allowing also forecaster expertise incorporation (Sénési et al. 2004). At DLR, a data fusion concept has been used for setting up and operationally implementing a system for diagnosing

atmospheric conditions for aircraft icing by combining surface and radar observations with forecast profiles of temperature and humidity (Tafferner et al. 2003).

Before describing the proposed integrated system, parts of which are already realized at DLR, we provide a complete summary of all tools in

Table 1. List of tools for an integrated system for weather nowcasting and forecasting: specified are data provider, area of observation, horizontal resolution, refresh rate, forecast horizon, form of output and comments as regards to the use of input data, abbreviations or specific explanation

| Tool/data source	Provider	Area	Resol.	Refresh rate (min)	Forecast horizon (h)	Output	Comments
Cloud-Tracker Cb-TRAM	DLR	Europe, UDC	2–4 km	15	1	Objects (IDL)	Use of MSG HRV, IR, WV channels, coded in IDL
Radar-Tracker Rad-TRAM*	DLR	Europe, UDC	2 km	15	1	Objects (IDL)	Use of European radar composite, coded in IDL
POLDIRAD	DLR	Part of UDC	~500 m	~10	Ana.	Reflect, Doppler veloc., ZDR, LDR, phiDP	Polarimetric Doppler Radar installed at DLR Oberpfaffenhofen, Germany
SYNPOLRAD	DLR	Part of UDC	Grid resol. of num. model	~10	Ana.	Synthetic reflectivity, LDR, ZDR on model grid	Synthetic Polarimetric Radar, provides input to image matcher for observed and synthetic radar images
NOWAIRE	DLR	UDC	2	10	3	Standard output, thunderstom indices, turbulence	Nowcasting Weather for Airport Environments, Combination of LM (DWD) with nested high-resolution model MM5/FSL
LME	DWD/ DLR	Europe, UDC	7 km	60	72	Gridded data	Standard output and fields related to convection, synthetic satellite observations for MSG
LM Ensemble	DWD/ DLR	Europe, UDC	7 km	60	72	Gridded data	Probability estimates, best member selection through image matcher
SYNSAT	DLR/ DWD	Europe, UDC	7 km	60	72	Synthetic satellite imagery	Provides input to image matcher
Image matcher	DLR	Europe	Pixel scale	–	–	Model forecast verification	Uses observed and synthetic satellite or radar imagery
VERA	IMG/ Uni-Wien	Part of middle Europe, includes UDC	20 km	60	Ana.	Gridded output, various analysis fields	Vienna Enhanced Resolution Analysis, for LM forecast verification and convection prone areas
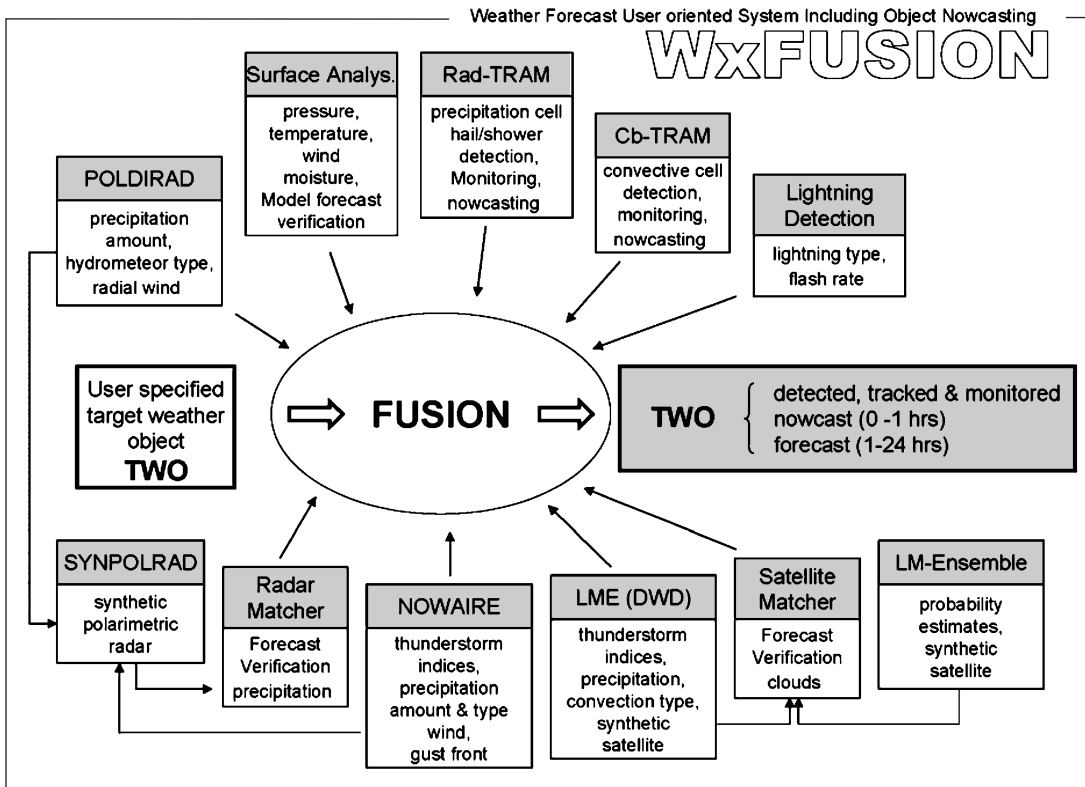
Fig. 14. Schematic depiction of the envisaged weather (Wx) fusion concept WxFUSION: user specified target weather objects (TWO; cf. Table 2) are filled with appropriate information through a fusion of selected nowcasting information (top half) and forecast products (bottom half)

Table 1. For each entry, the output products and space and time scales are listed.

All these tools are stand-alone applications which use one or more data sources. Furthermore, they produce output data which differ in type and format, a complication for the intended fusion of data which has to be handled by the integrated system. Figure 14 displays schematically the proposed system, called WxFUSION (weather fusion), an acronym which stands for "Weather Forecast User oriented System Including Object Nowcasting", with Wx being the standard acronym for weather in applications for aviation. The top row of tools in the figure all use observational data, surface observations as well as remote sensing, and are primarily used for nowcasting purpose. The bottom row consists of various forecasting models and tools for evaluating forecast performance. The core element FUSION reads the specification of a pre-defined *target weather object* (TWO) and fuses output data from the various tools in order to describe the weather object as well as possible. With regard of forecasting future states of the TWO, two time horizons are discriminated. Firstly, nowcasting up to one hour which primarily is based on the tools in the top line, and secondly, forecasting up to several hours based on the forecast tools as given in the bottom line. In order to clarify this process, the possible content of a TWO specified for thunderstorms is presented in Table 2 and a graphical representation of such an object is schematically displayed in Fig. 15.

As shown in Table 2 a TWO consists of descriptive parameters as well as weather elements. Here, possible parameters for a thunderstorm object are listed, as the horizontal extension and height of the object, its state, whether it is growing decaying, and the forecasted track. Weather elements attached to this TWO are e.g. heavy rain, hail, lightning flash rate, and for the forecast range, risk areas of heavy precipitation, hail or wind. Of course there can be several TWOs at a single time. For the nowcasting range the TWO's information content relies solely on observational data: e.g. cloud parameters as detected from METOSAT8 satellite, precipitation and hydrometeor information from radar (European radar

Table 2. List of parameters for a target weather object TWO, exemplified for a thunderstorm object. Tools providing the parameters (conf. to Table 1) are given in brackets

Descriptive parameters	Identification (triggering location and time; Cb-TRAM)
	Size (extent, horiz., vert., Cb-TRAM, Rad-TRAM, POLDIRAD)
	State and type (convective, growing, decaying; Cb-TRAM, Rad-TRAM)
	Track (detected and nowcast; Cb-TRAM, Rad-TRAM)
	Cloud top temperature (Cb-TRAM)
	Cloud base (SYNOP, surface analysis)
Weather elements for nowcasting (0–1 h)	Heavy rain (Radar composite, POLDIRAD, SYNOP)
	Hail (Radar composite, POLDIRAD)
	Wind shear, turbulence (POLDIRAD, NOWAIRE)
	Lightning flash rate (network)
Weather elements for forecasting (1–12 h)	Risk areas for heavy precipitation and hail (LM, LMK NOWAIRE, Image Matching)
	Precipitation (LM, LMK NOWAIRE, Image Matching)
	Squall lines, wind shift lines (LMK, MM5, Image Matching)
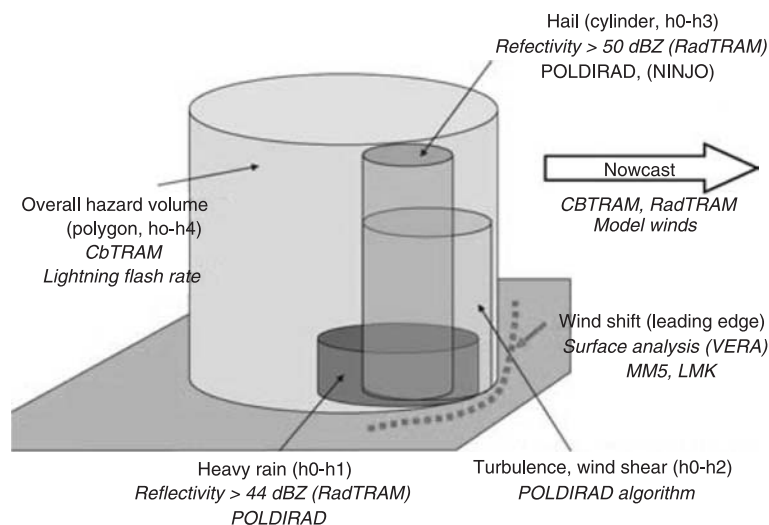
Fig. 15. Schematic geometrical structure of a *target weather object* (TWO); see text for details

composite and POLDIRAD operated by DLR), observations of lightning density (lightning networks like BLIDS, SAFIR and LINET) and surface analyses (e.g. VERA). For the longer time range the strategy will be that for each detected TWO (by Cb-TRAM and Rad-TRAM) the model forecasts are checked by making use of a forecast quality measure (like the one described in Sect. 4.4) whether they are able to capture the actual development. If the image matcher for observed and synthetic satellite and radar images found reasonable agreement of forecast and observation, the forecast can be used to provide information for the weather object for later hours.

We have to keep in mind, however, that this forecast information will not be as precise as the content of the nowcast information for the TWO which solely relies on observations. Also one can

expect that only in rare cases a model forecast will exactly match the observation. Therefore, one may concentrate only on the best forecast out of an ensemble and take displacements of weather objects in the forecast, i.e. phase errors, into account.

Figure 15 provides a visual imagination of such an object. The size of the TWO could be given by an overall hazard volume, e.g. the area of mature convection identified by the cloud tracker Cb-TRAM together with the detected cloud top temperature height. The latter can be calculated with the aid of background information, e.g. from of model forecast or a nearby radiosonde measurement (note that ECMWF tropopause data are already used in Cb-TRAM). The detected lightning flash rate observed within this volume would be attached as weather parameter to this

volume. Inside the overall hazard volume, observations of polarimetric radar will allow to determine finer scale volumes, as for hail, turbulence and heavy precipitation. Here, of course, certain thresholds have to be prescribed, e.g. as indicated in the figure for the hail volume. Furthermore, the leading edge of a moving thunderstorm system could be identified from surface analyses or high resolution model forecasts. Such a line is drawn in Fig. 4 deduced from the surface analysis of wind in the VERA system. All data belonging to one TWO can be packed into a specified format, ideally one which is well suited for objects, e.g. BUFR or XML, and distributed to users.

Of course, WxFUSIOM can also make use of redundant information, e.g. forecast tracks of the cloud and the radar tracker. If the tracks agree, the future positions of the TWO can be forecasted for the next hour with high confidence. Also probabilistic measures may be assigned to the tracks or future positions. As the image matching tool identifies forecast errors (cf. Sect. 4.4) it could be used to assign a confidence value to the current model forecast. A highly useful application of this technique would also be to determine the best forecast out of an ensemble as described in Tafferner et al. (2002) and then take the output of this forecast for the extended forecast range, e.g. rain amount, wind strength, and convective activity. Forecast quality can also be estimated from the VERA analyses which provide difference charts between observation and the forecast and can, therefore, determine phase shifts.

In summary, a sophisticated combination of the tools and data within the integrated system WxFUSION should allow to detect and monitor specified target weather objects and to estimate their geometric and weather related parameters. Future states of the weather objects up to one hour are provided by the nowcasting tools, e.g. in time intervals of 15 min and with an update rate of 15 min, the latter being dependent on the availability of satellite and radar data. As the quality of forecast mesoscale weather complexes is expected to degrade strongly already within the first hour, a high update rate is necessary to assure high quality products within this period. This requirement is much sought by several user groups, e.g. from aviation, where nowcasts for the next 20 min have to be as precise as possible

for airport operations while longer term forecasts should at least be precise enough to aid in strategic decision making, as e.g. opening or closing arrival gates. With regard to forecasting, the development and tracking of TWOs beyond the nowcasting range has to be based on model output data. Here it has to be assured that the forecast at hand is in accord with the observations as identified by image matching of observed and synthetic satellite and radar data. It is anticipated that the unifying vision of WxFUSION will be both useful and profitable during the inter-disciplinary project 'Weather and Aviation', which started in 2008.

References

Bergeron T (1928) Über die dreidimensional verknüpfende Wetteranalyse. Erster Teil: Prinzipielle Einführung in das Problem der Luftmassen- und Frontenbildung (On the three-dimensional interlinking weather analysis. First part: Basic introduction to the problem of air-mass and front generation). Geof Publ 5(6): 111pp

Cegnar T, Rakovec J (eds) (2005) International Workshop on Timely Warnings of Heavy Precipitation Episodes and Flash Floods. A collection of 10 essays with Slovenia as geographical focus. Special publication, Slovenian Meteorological Society, Ljubljana, 114pp

Dixon M, Wiener G (1993) TITAN: Thunderstorm identification, tracking, analysis, and nowcasting – a radar-based methodology. J Atmos Ocean Tech 10: 785–97

Doms G, Schättler U (1999) The Nonhydrostatic Limited Area Model LM (Lokal Modell) of DWD: Part I: Scientific Documentation. Deutscher Wetterdienst, Offenbach, 172pp

Evans JE, Ducot ER (1994) The Integrated Terminal Weather System (ITWS). Lincoln Lab J 7(2): 449–74

Frech M, Holzäpfel F, Tafferner A, Gerz T (2007) High-resolution weather database for the terminal area of frankfurt airport. J Appl Meteor Clim 46: 1913–32

Gerz T, Holzäpfel F, Bryant W, Köpp F, Frech M, Tafferner A, Winckelmans G (2005) Research towards a wake-vortex advisory system for optimal aircraft spacing. C R Physique 6: 501–23; DOI: 10.1016/j.crhy.2005.06.002

Grell GA, Emeis S, Stockwell WR, Schoenemeyer T, Forkel T, Michalakes J, Knoche R, Seidl W (2000) Application of

a multiscale, coupled MM5/chemistry model to the complex terrain of the VOTALP valley campaign. Atmos Environ 34: 1435–53

Hagen M, Schiesser H-H, Dorninger M (2000) Monitoring of mesoscale precipitation systems in the Alps and the northern Alpine foreland by radar and rain gauges. Meteorol Atmos Phys 72: 87–100

Handwerker J (2002) Cell tracking with TRACE3D – a new algorithm. Atmos Res 61: 15–34

Keil C, Craig GC (2007) A displacement-based error measure applied in a regional ensemble forecasting system. Mon Wea Rev 135: 3248–59

Keil C, Volkert H (2000) Precipitation in the northern Alpine region: Case-study-type validation of an operational forecast model. Meteorol Atmos Phys 72: 161–73

Kober K, Tafferner A (2008) Tracking and nowcasting of convective cells using remote sensing data from radar and satellite. Meteorol Z (submitted)

Koppert H-J (2002) A Java based meteorological workstation. 18th Internat. Conf. on Interactive Information and Processing Systems for Meteorology, Oceanography and Hydrography, Amer Meteorol Soc, Boston, pp. 307–10

Kron W (2004) Hochwasser. In: Wirtz A (ed) Wetterkatastrophen und Klimawandel (Weather catastrophies and climate change), Edition Wissen, Münchener Rückversicherungs-Gesellschaft, Order no. 302-04220, pp. 122–31

Morel C, Sénési S (2002) A climatology of mesoscale convective systems over Europe using satellite infrared imagery. I: Methodology. Quart J Roy Meteorol Soc 128: 1953–71

Mueller C, Saxen T, Roberts R, Wilson J, Betancourt T, Dettling S, Oien N, Yee J (2003) NCAR Auto-nowcast system. Wea Forecast 18: 545–61

Muller J-P, Denis M-A, Dundas RD, Mitchell KL, Naud C, Mannstein H (2007) Stereo cloud-top heights and cloud amount retrieval from ATSR2. Int J Remote Sensing 28: 1921–38; DOI: 10.1080/01431160601030975

Ranzi R, Zappa M, Bacchi B (2007) Hydrological aspects of the mesoscale alpine programme: findings from field experiments and simulations. Quart J Roy Meteorol Soc 133: 867–80

Sénési S, Morel C, Brovelli P, Arbogast E, Autones F, Bernard-Bouissières I, Bouzom M, Reynaud J (2004) Objectoriented convection nowcasting – using radar and satellite data in a man-machine mix. Proc. 3rd European Conference on Radar Meteorology and Hydrology, 6–10 September, Visby, Sweden

Steinacker R, Dorninger M, Wölfelmaier F, Krennert T (2000a) Automatic tracking of convective cells and cell complexes from lightning and radar data. Meteorol Atmos Phys 72: 101–10

Steinacker R, Haeberli C, Pöttschacher W (2000b) A transparent method for the analysis and quality evaluation of irregularly distributed and noisy observational data. Mon Wea Rev 128: 2303–16

Steppeler J, Doms G, Schättler U, Bitzer HW, Gassmann A, Damrath U, Gregoric G (2003) Meso-gamma scale forecasts using the nonhydrostatic model LM. Meteorol Atmos Phys 82: 75–96

Tafferner A, Hauf T, Leifeld C, Hafner T, Leykauf H, Voigt U (2003) ADWICE-advanced diagnosis and warning system for aircraft icing environments. Wea Forecast 18: 184–203

Tafferner A, Mannstein H, Paccagnella T, Marsigli C, Montani A, Nerozzi F (2002) On finding the best forecast out of an ensemble by satellite image matching for MAP IOP2b. 10th AMS Conf. on Mountain Meteor., Proc. Vol. pp. 201–4

Volkert H (2000) Heavy precipitation in the Alpine Region (HERA): Areal rainfall determination for flood warnings through in-situ measurements, remote sensing and atmospheric modelling. Meteorol Atmos Phys 72: 73–85

Volkert H, Gutermann T (2007) Inter-domain cooperation for mesoscale atmospheric laboratories: The Mesoscale Alpine Programme as a rich study case. Quart J Roy Meteorol Soc 133: 949–67

Volkert H, Weickmann L, Tafferner A (1991) The papal front of 3 May 1987: A remarkable example of frontogenesis near the Alps. Quart J Roy Meteorol Soc 117: 125–50

Wilson JW, Crook NA, Mueller CK, Sun J, Dixon M (1998) Nowcasting thunderstorms: a status report. Bull Amer Meteor Soc 79: 2079–99

Zinner T, Mannstein H, Tafferner A (2008) Cb-TRAM: tracking and monitoring severe convection from onset over rapid development to mature phase using multi-channel Meteosat-8 SEVIRI data. Meteorol Atmos Phys (in print)